

# Green Chemistry

Accepted Manuscript



This article can be cited before page numbers have been issued, to do this please use: W. Bing, H. Wang, L. Zheng, D. Rao, Y. Yang, L. Zheng, B. Wang, Y. Wang and M. Wei, *Green Chem.*, 2018, DOI: 10.1039/C8GC00851E.



This is an Accepted Manuscript, which has been through the Royal Society of Chemistry peer review process and has been accepted for publication.

Accepted Manuscripts are published online shortly after acceptance, before technical editing, formatting and proof reading. Using this free service, authors can make their results available to the community, in citable form, before we publish the edited article. We will replace this Accepted Manuscript with the edited and formatted Advance Article as soon as it is available.

You can find more information about Accepted Manuscripts in the [author guidelines](#).

Please note that technical editing may introduce minor changes to the text and/or graphics, which may alter content. The journal's standard [Terms & Conditions](#) and the ethical guidelines, outlined in our [author and reviewer resource centre](#), still apply. In no event shall the Royal Society of Chemistry be held responsible for any errors or omissions in this Accepted Manuscript or any consequences arising from the use of any information it contains.



## Green Chemistry

## ARTICLE

## CaMnAl-hydrotalcite solid basic catalyst toward aldol condensation reaction with a comparable level to liquid alkali catalysts

Received 00th January 20xx,  
Accepted 00th January 20xx

DOI: 10.1039/x0xx00000x

www.rsc.org/

Weihan Bing,<sup>a</sup> Huimin Wang,<sup>a</sup> Lei Zheng,<sup>b</sup> Deming Rao,<sup>a</sup> Yusen Yang,<sup>a</sup> Lirong Zheng,<sup>\*b</sup> Bin Wang,<sup>c</sup> Yangdong Wang<sup>\*d</sup> and Min Wei<sup>\*a</sup>

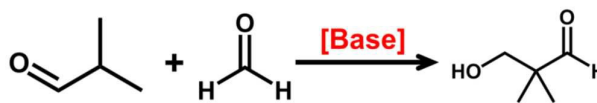
In a number of heterogeneous catalysis processes, promotion effect toward active sites is of vital importance and remains a challenge to obtain largely-improved catalytic performance. Herein, rehydrated Ca<sub>4</sub>Mn<sub>x</sub>Al-layered double hydroxides (denoted as re-Ca<sub>4</sub>Mn<sub>x</sub>Al-LDH) were prepared based on a structure memory effect of LDH precursors, which exhibited extremely high heterogeneous catalytic performance for aldol condensation reaction, with the assistance of promotion effect of Mn. A combination study including XRD, EXAFS, XPS, CDCl<sub>3</sub>-FTIR and DFT calculations confirms that re-Ca<sub>4</sub>Mn<sub>x</sub>Al-LDH samples with Ca–O–Mn<sup>IV</sup> structure show a highly-exposed Ca<sup>2+</sup> s-orbital and strengthened coordination between Ca<sup>2+</sup> with 7-fold OH<sup>−</sup>, providing a weakened Brønsted basic site compared with the reference sample re-Ca<sub>4</sub>Al-LDH. The optimized re-Ca<sub>4</sub>Mn<sub>0.5</sub>Al-LDH catalyst exhibits prominent catalytic performance toward the condensation of isobutyraldehyde (IBD) and formaldehyde (FA) to produce hydroxypivaldehyde (HPA), with a HPA yield of 70.3%. This is significantly higher than re-Ca<sub>4</sub>Al-LDHs (63.3%) and even comparable to the level of liquid alkali catalysts (73.2%). Studies on the structure-property correlation reveal that the weakened basic site originating from Ca–O–Mn<sup>IV</sup> serves as a promoted active center, which accelerates the product desorption and thus largely improves HPA selectivity. This promoted re-Ca<sub>4</sub>Mn<sub>0.5</sub>Al-LDH catalyst can be potentially applied as a promising candidate in heterogeneous aldol condensation reactions.

### 1. Introduction

Aldol condensation is a well-known and important C–C coupling reaction in classic organic synthesis via reaction between aldehydes and/or ketones, which produces a variety of value-added chemicals with versatile commercial applications (e.g., polymers, pharmaceuticals, and agricultural chemicals).<sup>1–3</sup> Herein, the aldol condensation of isobutyraldehyde (IBD) with formaldehyde (FA) to produce hydroxypivaldehyde (HPA) (Scheme 1), as a base-catalyzed reaction with great industrial importance, has been widely applied in the production of polyesters, plasticizers, synthetic resin paints and lubricants. Traditionally, this aldol reaction is catalysed by homogeneous bases (e.g., aqueous NaOH, KOH, and triethylamine), which suffers from a number of disadvantages including generation of waste liquid, environmental pollution and equipment corrosion.<sup>4–6</sup> Therefore, heterogeneous base catalysis plays a more

pivotal role, as their applications in many base-catalyzed industrial processes offer opportunities to facilitate separation, avoid corrosion and pollution issue.<sup>7–9</sup> Recently, for the aldol condensation of IBD with FA towards HPA, a series of perovskites and metal nitrides as heterogeneous base catalysts have been reported. However, these solid basic catalysts suffer from a very sluggish development both in fundamental study and industrial application, owing to great challenges in material exploration and technique limitation.

By virtue of the advantages of layered double hydroxides (LDHs) including versatile chemical composition and structural memory effect, the rehydrated CaAl-LDHs as an effective solid basic catalyst was prepared for this aldol reaction in our previous work;<sup>10</sup> moreover, it has been verified that the 7-fold Ca–OH coordination structure with weak Brønsted basic site accelerates the desorption of aldol condensation product, which is the key step to enhance the selectivity toward HPA. Although rehydrated CaAl-LDHs (re-CaAl-LDHs) as a new solid basic catalyst toward aldol condensation reaction has been developed, its catalytic performance is not as high as the level of liquid alkali catalysts, and a control over fine structure of Ca–O–Al (weak Brønsted basic site structure) is highly



Scheme 1 Base-catalysed aldol condensation of IBD with FA towards HPA.

<sup>a</sup> State Key Laboratory of Chemical Resource Engineering, Beijing Advanced Innovation Center for Soft Matter Science and Engineering, Beijing University of Chemical Technology, Beijing 100029, P. R. China. E-mail: weimin@mail.buct.edu.cn

<sup>b</sup> Institute of High Energy Physics, the Chinese Academy of Sciences, Beijing 100049, P. R. China. E-mail: zhenglr@ihep.ac.cn

<sup>c</sup> Beijing Research Institute of Chemical Industry, Sinopec Group, Beijing 100013, P. R. China.

<sup>d</sup> SINOPEC Shanghai Research Institute of Petrochemical Technology, Shanghai 201208, P. R. China. E-mail: wangyd.sshy@sinopec.com

†Electronic Supplementary Information (ESI) available: See DOI:

necessary for a further improvement. In the past decades, many elements, such as lanthanum, cerium, zirconium and manganese have been investigated as promoters to enhance catalytic performance toward aldol condensation reactions; among these promoters, manganese as an effective promoter has attracted considerable attention, due to its versatile valence state and electronic structure. On the other hand, based on our previous understanding, if the active basic site could be tuned *via* changing the electronic structure of Ca–O–Al, a further promotion of catalytic performance would be achieved. Therefore, partial substitution of Al by another metal element with special M–O bonding (*e.g.*, Mn<sup>IV</sup>–O) would modify the fine structure of basic site and therefore make a further enhancement of catalytic performance toward aldol condensation reaction.

Inspired by the above idea, herein, on the basis of rehydrated CaAl-LDHs, Mn element was further introduced to prepare rehydrated CaMnAl-LDHs solid base catalyst, which was used in aldol condensation of isobutyraldehyde (IBD) with formaldehyde (FA) to produce hydroxypivalaldehyde (HPA). Among them, the optimized re-Ca<sub>4</sub>Mn<sub>0.5</sub>Al-LDH sample shows an extremely high catalytic performance with a HPA yield of 70.3%, significantly higher than re-Ca<sub>4</sub>Al-LDHs (63.3%) and even comparable to the level of liquid alkali catalysts (73.2%). A combination study including XRD, EXAFS, and XPS confirms that low Mn-containing samples (Mn/Al molar ratio: 0.3, 0.5) involve predominant Mn<sup>IV</sup> species; the resulting Ca–O–Mn<sup>IV</sup> structure with a highly-exposed Ca<sup>2+</sup> s-orbital and strengthened interaction with 7-fold OH<sup>−</sup>, provides a weakened Brønsted basic site revealed by deuterated chloroform–FTIR spectra. In contrast, high Mn-containing samples (Mn/Al molar ratio from 0.8 to 1.5) possess abundant Ca–O<sub>v</sub>–Mn<sup>III</sup> structure (O<sub>v</sub> denotes oxygen vacancy) with a decreased interaction between Ca<sup>2+</sup> and 7-fold OH<sup>−</sup>, giving rise to medium Brønsted basic site. By establishing the correlation between catalytic performance and relative concentration of Mn species, it is found that the weakened basic site originating from Ca–O–Mn<sup>IV</sup> facilitates the product desorption and inhibits further polycondensation, accounting for the significantly enhanced HPA yield over re-Ca<sub>4</sub>Mn<sub>0.5</sub>Al-LDH. DFT calculations reveal that Ca–O–Mn<sup>IV</sup> structure gives a lattice expansion and a shortened 7-fold Ca–O bond, which induces a weakened basic site and a markedly decreased desorption energy of HPA (0.179 eV) relative to pristine Ca–O–Al structure (0.557 eV). This work demonstrates a successful paradigm for the enhancement of LDHs-based solid base catalyst by introducing promoter Mn<sup>IV</sup>, and provides an in-depth understanding on the promotion mechanism of Ca–O–Mn<sup>IV</sup>.

## 2. Experiment Section

### 2.1 Materials

Chemical reagents, including Ca(NO<sub>3</sub>)<sub>2</sub>•4H<sub>2</sub>O, Al(NO<sub>3</sub>)<sub>3</sub>•9H<sub>2</sub>O, Mn(NO<sub>3</sub>)<sub>2</sub> (50% aqueous solution), NaOH, isobutyraldehyde (IBD), formaldehyde (FA, 37% aqueous solution), dioxane, hydroxypivalaldehyde (HPA) and cetyl trimethyl ammonium bromide (CTAB) were purchased and used without further purification. Deionized and decarbonated water was used in all the experimental processes.

### 2.2 Preparation of catalysts

**Synthesis of Ca<sub>4</sub>Mn<sub>x</sub>Al-LDH precursor:** Ca<sub>4</sub>Al-LDH and Ca<sub>4</sub>Mn<sub>x</sub>Al-LDH precursors with varying Mn/Al molar ratios were synthesized using a coprecipitation method as follows. In a typical procedure, 0.04 mol of Ca(NO<sub>3</sub>)<sub>2</sub>•4H<sub>2</sub>O, 0.01 mol of Al(NO<sub>3</sub>)<sub>3</sub>•9H<sub>2</sub>O and Mn(NO<sub>3</sub>)<sub>2</sub> aqueous solution with a given Mn : Al molar ratio (0, 0.3, 0.5, 0.8, 1.0 and 1.5, respectively) were dissolved in deionized and decarbonated water (100 mL), which was then added simultaneously into a three-neck round-bottom flask with NaOH aqueous solution (100 mL, 1.1 M) in N<sub>2</sub> atmosphere. The precipitate was stirred vigorously at pH 12.6–13.2 at room temperature for 6 h, followed by separation, washing thoroughly and drying at 80 °C for 24 h.

**Synthesis of re-Ca<sub>4</sub>Mn<sub>x</sub>Al-LDH:** The rehydrated LDH catalysts were prepared in a two-step procedure. Firstly, 0.5 g of the as-synthesized LDH precursor was heated at 500 °C for 4 h in air atmosphere at a heating rate of 2 °C min<sup>−1</sup>. Subsequently, the calcination sample was cooled down to room temperature and then dispersed in a NaOH solution with stirring for 2 h. We chose an appropriate pH value of 13.40 for the preparation of rehydrated LDHs samples with a high purity. The obtained product was filtered, washed thoroughly with water and ethanol, finally dried at 80 °C for 12 h, labeled as re-Ca<sub>4</sub>Mn<sub>x</sub>Al-LDH (x=0, 0.3, 0.5, 0.8, 1.0 and 1.5).

### 2.3 Catalytic reaction

The aldol condensation reaction was carried out using a batch-type reactor (cylindrical glass tube), avoiding exposing the catalyst to air. Typically, the freshly prepared re-Ca<sub>4</sub>Mn<sub>x</sub>Al-LDH catalyst (0.2 g) was dispersed into a mixture of IBD (0.55 mol), FA (0.80 mol, 37% aqueous solution), dioxane (0.2 g, as internal standard) and CTAB (0.1 g) in Ar atmosphere. Herein CTAB is used as a phase transfer catalyst, which can facilitate the migration of IBD from oil phase into water phase to accelerate reaction, so as to obtain a high conversion and inhibit byproducts in oil-water two-phase reaction system. After vacuuming and inletting argon gas, the solution was magnetically stirred in oil bath at 70 °C. The power and rotating rate of magnetic stirrer were also studied to reduce the influence of mass transfer, and an optimized stirring condition (15 W, 600 r/min) was applied in this work. The reactant conversion and product yield were monitored by GC-2014 Shimadzu gas chromatograph (GC) equipped with a flame ionization detector (FID) and an Rtx-5 capillary column (0.25 mm in diameter, 30 m in length). The products were identified by gas chromatography–mass spectrometry (GC–MS) equipped with the same column as GC.

### 2.4 Characterization

X-ray diffraction (XRD) patterns were recorded on a Shimadzu XRD-6000 diffractometer, using Cu Kα radiation (λ = 0.1542 nm) at 40 kV, 30 mA. X-ray photoelectron spectra (XPS) were recorded on a Thermo VG Escalab 250 X-ray photoelectron spectrometer at a pressure of ~2 × 10<sup>−9</sup> Pa with Al Kα X-rays as the excitation source. Extend X-ray absorption fine structure spectroscopy (EXAFS) at the Mn and Ca K-edge was performed at the beamline 1W1B and 4B7A of the Beijing Synchrotron Radiation Facility (BSRF), Institute of High Energy Physics (IHEP), Chinese Academy of Sciences (CAS). For the Mn EXAFS, the typical energy of the storage ring was 2.5 GeV with a maximum current of 250 mA. The typical energy of the storage ring of Ca EXAFS was 2.2 GeV with a maximum current of 100 mA. The Si

(111) double crystal monochromator was used. The IFFEFIT 1.2.11 date analysis package (Athena, Artemis, Atoms, and FEFF6) was used for the date analysis.

Deuterated chloroform was used as a basicity probe molecule for the measurement of FTIR transmission spectroscopy, which was carried out in a Bruker Equinox 55 spectrometer, between 4000 and 400  $\text{cm}^{-1}$  with a resolution of 4  $\text{cm}^{-1}$  after 600 scans per spectrum. The nature of the basic site was characterized by the FTIR spectroscopy of adsorbed deuterated chloroform ( $\text{CDCl}_3$ -IR). About 18 mg of sample was pressed into a wafer with a diameter of 1.3 cm, installed in an IR cell with  $\text{CaF}_2$  windows, treated at 150  $^\circ\text{C}$  for 0.5 h, followed by an evacuation treatment at this temperature. Subsequently, the sample was cooled to 50  $^\circ\text{C}$  for recording the background spectrum. With the introduction of deuterated chloroform into the cell for 1 h, another evacuation was performed to remove physisorbed deuterated chloroform; afterwards, the spectrum was recorded with a step of 4  $\text{cm}^{-1}$  and an accumulation of 32 scans. The strength of base site involved in the adsorption of  $\text{CDCl}_3$  was estimated based on the following equation:

$$\log \Delta \nu_{\text{CD}} = 0.0066 \text{PA} - 4.36 \quad (1)$$

where  $\Delta \nu_{\text{CD}}$  is the shift of  $\nu_{\text{CD}}$  ( $\text{cm}^{-1}$ ), and PA is the proton affinity ( $\text{kJ mol}^{-1}$ ).

## 2.5 Computational methods

The density functional theory calculations were performed with the Vienna Ab-initio Simulation Package (VASP) in slab models. The model of  $\text{CaMnAl-OH-LDH}$  was constructed according to the crystal data of these LDHs reported previously. The space group of LDHs was  $r\bar{3}m$ , with unit cell parameters  $\alpha = \beta = 90^\circ$ , and  $\gamma = 120^\circ$ . The other three unit cell parameters  $a$ ,  $b$  and  $c$ , are referred to the powder X-ray diffraction data of these LDHs. The supercell of bulk  $\text{CaMnAl-LDH}$  is set to be  $3 \times 3 \times 1$  in the  $a$ -,  $b$ -, and  $c$ -direction with the accustomed molar ratio of  $\text{Ca} : \text{Mn} : \text{Al} = 4 : 1 : 1$ . Three hydroxyl ions were placed into the interlayer gallery of bulk  $\text{Ca}_4\text{Mn}_1\text{Al}_1\text{-LDH}$  to keep the charge neutral. The exchange-correlation potential was described by the Perdew-Burke-Ernzerhof (PBE) in generalized gradient approach (GGA). The structure optimizations were based on the following points: (1) an energy tolerance of  $1.0 \times 10^{-4}$  eV per atom; (2) a maximum force tolerance of 0.2 eV; (3) the  $k$ -points were set to be  $3 \times 3 \times 1$  in calculating the electronic structure.

## 3. Results and discussion

### 3.1 Structural and morphological characterizations

The rehydrated  $\text{Ca}_4\text{Mn}_x\text{Al-LDH}$  solid basic catalysts with various  $\text{Mn}/\text{Al}$  ratios ( $x=0, 0.3, 0.5, 0.8, 1.0, 1.5$ ) were prepared via a facile coprecipitation method, followed by a calcination and a rehydration process in an aqueous  $\text{NaOH}$ . XRD patterns of  $\text{Ca}_4\text{Mn}_x\text{Al-LDH}$  precursors (Fig. S1A) and the calcination samples  $\text{Ca}_4\text{Mn}_x\text{Al-MMO}$  (Fig. S1B) show a series of reflections indexed to a characteristic feature of layered  $\text{NO}^{3-}$ -containing LDH phase and  $\text{CaO}$ -periclase phase, respectively. As shown in Fig. 1, the rehydration samples (denoted as  $\text{re-Ca}_4\text{Mn}_x\text{Al-LDH}$ ) display characteristic peaks of an LDH phase, with the (003) reflection shifting to a higher  $2\theta$  relative to  $\text{NO}^{3-}$ -containing LDH precursor ( $11.5^\circ$  vs.  $10.5^\circ$ ). This indicates

the reconstruction of layered structure with  $\text{OH}^-$  as interlayer anion. Moreover, some weak peaks are observed in XRD patterns of  $\text{Ca}_4\text{Mn}_x\text{Al-LDH}$  precursors and  $\text{re-Ca}_4\text{Mn}_x\text{Al-LDH}$  samples, attributed to the presence of a small amount of  $\text{CaCO}_3$  and manganese oxide phase ( $\text{Mn}_2\text{O}_3$  or  $\text{MnO}_2$ ). Correspondingly, the cell parameters of  $\text{re-Ca}_4\text{Mn}_x\text{Al-LDH}$  (listed in Table 1) are calculated based on (003) and (110) reflection as  $c = \sim 22.80 \text{ \AA}$  and  $a = \sim 3.32 \text{ \AA}$ , respectively, which are in accordance with the characteristics of  $\text{OH}^-$  intercalated  $\text{Ca}_4\text{Mn}_x\text{Al-LDH}$ . SEM images of these rehydrated LDH samples (Fig. S2) show plate-like microcrystals with a lateral diameter distribution of 1.0–2.0  $\mu\text{m}$ . Nitrogen adsorption-desorption isotherms of  $\text{re-Ca}_4\text{Mn}_x\text{Al-LDH}$  samples display comparable specific surface, average pore size and total pore volume (Table 1). Moreover, the molar ratios of  $\text{Ca}/\text{Mn}/\text{Al}$  of  $\text{Ca}_4\text{Mn}_x\text{Al-LDH}$  and  $\text{re-Ca}_4\text{Mn}_x\text{Al-LDH}$  samples determined by inductively coupled plasma-atomic emission spectrometer (ICP-AES) are also summarized in Table 1 and Table S1, which are close to the nominal values. The aluminium content in  $\text{re-Ca}_4\text{Mn}_x\text{Al-LDH}$  samples does not show obvious change after rehydration with  $\text{NaOH}$  solution, indicating rather less Al leaching.

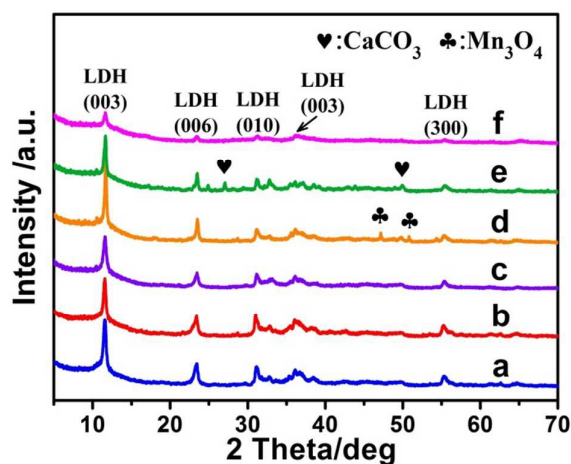


Fig. 1 XRD patterns of (a)  $\text{re-Ca}_4\text{Al-LDH}$ , (b)  $\text{re-Ca}_4\text{Mn}_{0.3}\text{Al-LDH}$ , (c)  $\text{re-Ca}_4\text{Mn}_{0.5}\text{Al-LDH}$ , (d)  $\text{re-Ca}_4\text{Mn}_{0.8}\text{Al-LDH}$ , (e)  $\text{re-Ca}_4\text{Mn}_{1.0}\text{Al-LDH}$  and (f)  $\text{re-Ca}_4\text{Mn}_{1.5}\text{Al-LDH}$ , respectively.

EXAFS spectroscopy was performed to investigate the detailed structure (Fig. 2), and the normalized Mn K-edge XANES spectra for these five  $\text{re-Ca}_4\text{Mn}_x\text{Al-LDH}$  samples and reference samples ( $\text{MnO}$ ,  $\text{Mn}_2\text{O}_3$  and  $\text{MnO}_2$ ) are shown in Fig. 2A. Pure  $\text{MnO}$  has the lowest absorption edge, followed by  $\text{Mn}_2\text{O}_3$ , and  $\text{MnO}_2$  displays the highest absorption edge. For all these  $\text{re-Ca}_4\text{Mn}_x\text{Al-LDH}$  samples, the edge position is located between  $\text{Mn}_2\text{O}_3$  and  $\text{MnO}_2$ , indicating the coexistence of trivalent manganese ( $\text{Mn}^{\text{III}}$ ) and tetravalent manganese ( $\text{Mn}^{\text{IV}}$ ) species,<sup>11–14</sup> which is also confirmed by UV-vis absorption spectroscopy (Fig. S3).<sup>15</sup> Notably, the absorption edge of  $\text{re-Ca}_4\text{Mn}_x\text{Al-LDH}$  samples shifts toward low photon energy with the increment of Mn content, indicating a reduced relative concentration of  $\text{Mn}^{\text{IV}}$  (Fig. 2A and inset). Moreover, as shown in fourier-transform EXAFS spectra at Mn K-edge (Fig. 2B), Mn–O distance in the first shell of  $\text{re-Ca}_4\text{Mn}_x\text{Al-LDH}$  samples is 1.48  $\text{Å}$ , the same to that of  $\text{Mn}_2\text{O}_3$  and  $\text{MnO}_2$ . It should be noted that the coordination number of Mn–O bond decreases obviously with the

enhancement of Mn/Al ratio, which suggests the existence of low-coordinated Mn–O structure such as oxygen vacancies (*i.e.*, Ca–O<sub>v</sub>–Mn<sup>III</sup>).

For the five re-Ca<sub>4</sub>Mn<sub>x</sub>Al-LDH samples and reference sample re-Ca<sub>4</sub>Al-LDH, Ca K-edge XANES spectra (Fig. 2C) the FT k<sub>3</sub>-weighted EXAFS spectra (Fig. 2D) are also studied. Fig. 2C shows a weak pre-edge feature at ~4043 eV corresponding to transitions from 1s to 3d state, which indicates the distorted 7-fold Ca<sup>2+</sup>–OH with a low structural symmetry existing in Ca-containing LDHs. With the increase of Mn/Al molar ratio, the photon energy of central peak (white line) decreases firstly and then increases, and the minimal photon energy (4052.0 eV) presents in the sample of re-Ca<sub>4</sub>Mn<sub>0.5</sub>Al-LDH (Fig. 2C). Depuyrot *et al.* has reported a positive correlation between mean oxidation state of metal cation and photon energy.<sup>16</sup> Herein, we used the similar method to estimate mean oxidation

state and average electron density of Ca<sup>2+</sup> in re-Ca<sub>4</sub>Mn<sub>x</sub>Al-LDH samples. As the Mn/Al ratio increases from x=0 to x=0.5, the average electron density of Ca<sup>2+</sup> increases and reaches the maximal value in re-Ca<sub>4</sub>Mn<sub>0.5</sub>Al-LDH sample; meanwhile, as shown in fourier-transform EXAFS spectra at Ca K-edge (Fig. 2D), the Ca–O distance in re-Ca<sub>4</sub>Mn<sub>0.5</sub>Al-LDH (~1.90 Å) is obviously longer than that in re-Ca<sub>4</sub>Al-LDH (~1.82 Å), indicating a lattice expansion of Ca–O–Mn<sup>IV</sup> octahedron. This lattice expansion induces an enhanced exposure of Ca<sup>2+</sup> s-orbital and thus strengthens the interaction between Ca<sup>2+</sup> and the 7-fold OH<sup>–</sup> (OH<sup>–</sup> group as an electron donor), which increases the average electron density of Ca<sup>2+</sup>. In addition, from x=0.5 to x=1.5, Ca–O distance becomes shorter with a reduced coordination number (Fig. 2D), which indicates the existence of Ca–O<sub>v</sub>–Mn<sup>III</sup> structure, in accordance with the results of Mn K-edge EXAFS spectroscopy.

**Table 1. Physicochemical Properties of re-Ca<sub>4</sub>Mn<sub>x</sub>Al-LDH samples**

Sample	Ca/Mn/Al molar ratio <sup>a</sup>	BET surface area (m <sup>2</sup> g <sup>–1</sup> )	Pore diameter (nm)	Total pore volume (cm <sup>3</sup> g <sup>–1</sup> )	c (Å) <sup>b</sup>	a (Å) <sup>c</sup>
re-Ca <sub>4</sub> Al-LDH	3.94 : 0.00 : 1	28.2	7.4	0.139	22.98	3.32
re-Ca <sub>4</sub> Mn <sub>0.3</sub> Al-LDH	3.92 : 0.26 : 1	34.3	7.9	0.191	22.90	3.33
re-Ca <sub>4</sub> Mn <sub>0.5</sub> Al-LDH	3.98 : 0.51 : 1	26.5	10.3	0.220	22.82	3.32
re-Ca <sub>4</sub> Mn <sub>0.8</sub> Al-LDH	3.91 : 0.87 : 1	33.3	9.5	0.225	22.70	3.32
re-Ca <sub>4</sub> Mn <sub>1.0</sub> Al-LDH	3.91 : 1.11 : 1	22.1	12.3	0.318	22.78	3.31
re-Ca <sub>4</sub> Mn <sub>1.5</sub> Al-LDH	3.99 : 1.64 : 1	29.6	11.6	0.426	22.82	3.31

<sup>a</sup> Ca/Mn/Al molar ratio was measured by inductively coupled plasma–atomic emission spectroscopy (ICP–AES). <sup>b</sup> Lattice parameter *a* was determined by the formula  $a = 2d110$ , which is related to the average cation–cation distance in the brucite-like sheets. <sup>c</sup> Lattice parameter *c* was determined by the formula  $c = 3d003$ , which is indicative of interlayer distance.

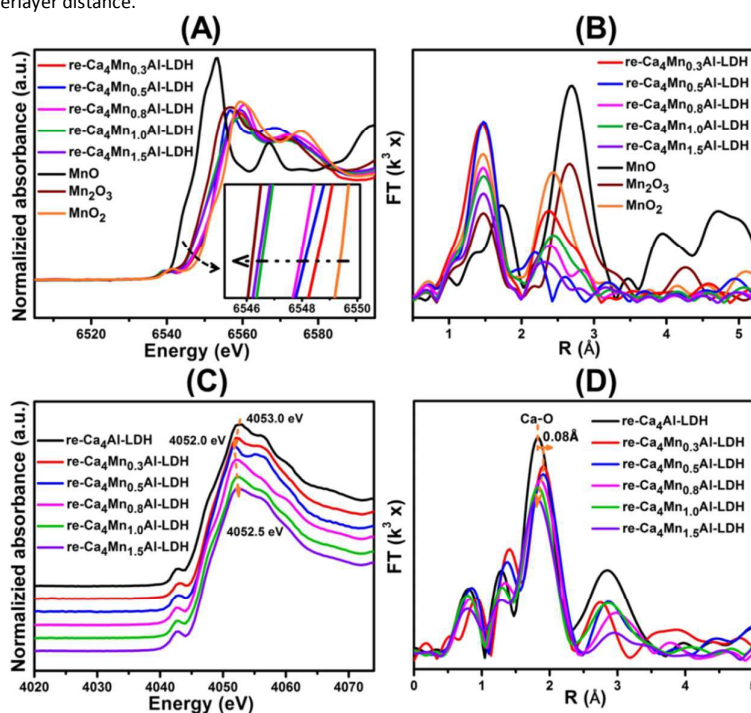


**Fig. 2** (A) Normalized XANES spectra and (B) Fourier-transform EXAFS spectra at Mn K-edge for re-Ca<sub>4</sub>Mn<sub>0.3</sub>Al-LDH, re-Ca<sub>4</sub>Mn<sub>0.5</sub>Al-LDH, re-Ca<sub>4</sub>Mn<sub>0.8</sub>Al-LDH, re-Ca<sub>4</sub>Mn<sub>1.0</sub>Al-LDH, re-Ca<sub>4</sub>Mn<sub>1.5</sub>Al-LDH, MnO, Mn<sub>2</sub>O<sub>3</sub> and MnO<sub>2</sub>, respectively; inset: the enlarged view of absorption edge selected from (A). (C) Normalized XANES spectra and (D) Fourier-transform EXAFS spectra at Ca K-edge for re-Ca<sub>4</sub>Al-LDH, re-Ca<sub>4</sub>Mn<sub>0.3</sub>Al-LDH, re-Ca<sub>4</sub>Mn<sub>0.5</sub>Al-LDH, re-Ca<sub>4</sub>Mn<sub>0.8</sub>Al-LDH, re-Ca<sub>4</sub>Mn<sub>1.0</sub>Al-LDH and re-Ca<sub>4</sub>Mn<sub>1.5</sub>Al-LDH, respectively.

XPS spectra of Mn2p and O1s for these re-Ca<sub>4</sub>Mn<sub>x</sub>Al-LDH samples were investigated, so as to further quantify Mn species and explore the electronic structure of O species. Fig. 3A shows the spin-orbit splitting of Mn2p<sub>1/2</sub> and Mn2p<sub>3/2</sub> signals for re-Ca<sub>4</sub>Mn<sub>x</sub>Al-LDH samples. The broad, asymmetric Mn2p<sub>3/2</sub> peak can be deconvoluted into two symmetry peaks centered at ~642.15 and 643.45 eV, which are assigned to Mn<sup>III</sup> and Mn<sup>IV</sup> species, respectively.<sup>17–19</sup> With the increment of Mn content, the Mn<sup>IV</sup>/Mn<sup>III</sup> molar ratio in re-Ca<sub>4</sub>Mn<sub>x</sub>Al-LDH samples estimated from the peak intensities decreases significantly (Fig. 3A and Table 2), which is indicative of the gradual transformation from Ca–O–Mn<sup>IV</sup> to Ca–O<sub>v</sub>–Mn<sup>III</sup> structure. Moreover, Mn3s spectra of re-Ca<sub>4</sub>Mn<sub>x</sub>Al-LDH samples were collected to determine the average oxidation state of Mn cations (Fig. S4). As has been reported, the Mn average oxidation state (AOS) can be determined through the exchange splitting of Mn3s spectra ( $\Delta E_{3s}$ ) according to the linear equation:  $AOS = 8.956 - 1.13 (\Delta E_{3s})$ .<sup>20–21</sup> Therefore, except re-Ca<sub>4</sub>Mn<sub>0.3</sub>Al-LDH without observed Mn3s peak, AOS of Mn species decreases in the following sequence: re-Ca<sub>4</sub>Mn<sub>0.5</sub>Al-LDH (4.75) > re-Ca<sub>4</sub>Mn<sub>0.8</sub>Al-LDH (4.68) > re-Ca<sub>4</sub>Mn<sub>1.0</sub>Al-LDH (4.57) > re-Ca<sub>4</sub>Mn<sub>1.5</sub>Al-LDH (4.50). This indicates that the relative concentration of Mn<sup>IV</sup> decreases along with the increment of Mn content, in accordance with the results of Mn K-edge XANES spectroscopy.

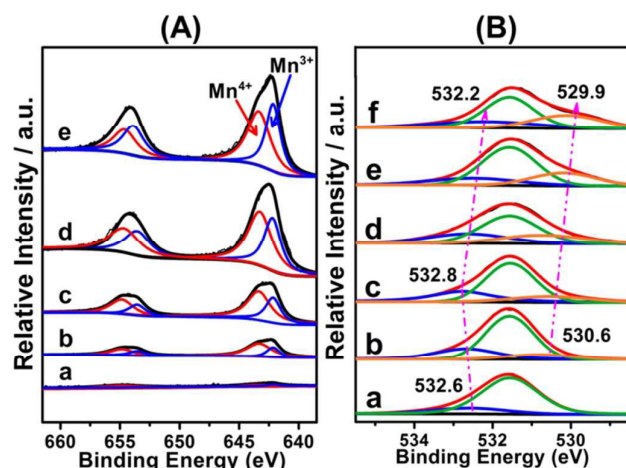


**Fig. 3** (A) XPS Mn2p of (a) re-Ca<sub>4</sub>Mn<sub>0.3</sub>Al-LDH, (b) re-Ca<sub>4</sub>Mn<sub>0.5</sub>Al-LDH, (c) re-Ca<sub>4</sub>Mn<sub>0.8</sub>Al-LDH, (d) re-Ca<sub>4</sub>Mn<sub>1.0</sub>Al-LDH and (e) re-Ca<sub>4</sub>Mn<sub>1.5</sub>Al-LDH. (B) XPS O1s of (a) re-Ca<sub>4</sub>Al-LDH, (b) re-Ca<sub>4</sub>Mn<sub>0.3</sub>Al-LDH, (c) re-Ca<sub>4</sub>Mn<sub>0.5</sub>Al-LDH, (d) re-Ca<sub>4</sub>Mn<sub>0.8</sub>Al-LDH, (e) re-Ca<sub>4</sub>Mn<sub>1.0</sub>Al-LDH and (f) re-Ca<sub>4</sub>Mn<sub>1.5</sub>Al-LDH.

Fig. 3B shows a broad O1s spectrum within 528.8–535.2 eV, which are deconvoluted to three peaks by Gaussian peak fitting method for these re-Ca<sub>4</sub>Mn<sub>x</sub>Al-LDH samples. The two peaks at ~532.6 eV and ~531.6 eV are assigned to surface hydroxyl in 7-fold Ca–OH coordination and Ca–O–Al lattice oxygen species in brucite-like layers of edge-sharing Ca(OH)<sub>6</sub> octahedron; whilst the peak ~530.6 eV is attributed to the Ca–O–Mn lattice oxygen species. With the increase of Mn/Al molar ratio from 0.3 to 0.5, the peak of oxygen species in 7-fold Ca–OH coordination shifts to higher binding energy (532.7 eV and 532.8 eV) relative to re-Ca<sub>4</sub>Al-LDH reference (532.6 eV), and then shifts to lower binding energy (532.2 eV) with the Mn/Al molar ratio from 0.5 to 1.5. The results indicate that for the low Mn-containing samples (Mn/Al molar: 0.3, 0.5), the

dominant Ca–O–Mn<sup>IV</sup> structure induces a strengthened 7-fold Ca–OH coordination and therefore a low electron density of hydroxyl oxygen species; in contrast, for samples with Mn/Al molar ratio from 0.5 to 1.5, the predominant Ca–O<sub>v</sub>–Mn<sup>III</sup> structure leads to a weakened 7-fold Ca–OH coordination with a high electron density of hydroxyl oxygen species, in accordance with Ca XANES spectra. In addition, the deconvoluted peak due to Ca–O–Mn lattice oxygen species becomes augmented and shifts toward lower binding energy as the Mn/Al molar ratio increases from  $x=0$  to  $x=1.5$ , which could be attributed to the electron transfer from Mn<sup>III</sup> (with a higher electron density relative to Mn<sup>IV</sup>) to adjacent lattice oxygen.

### 3.2 Surface basic properties of re-Ca<sub>4</sub>Mn<sub>x</sub>Al-LDH samples

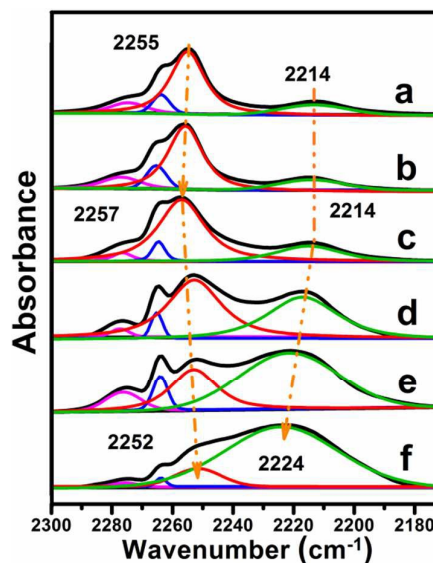


**Fig. 4** FTIR transmission spectra of (a) re-Ca<sub>4</sub>Al-LDH, (b) re-Ca<sub>4</sub>Mn<sub>0.3</sub>Al-LDH, (c) re-Ca<sub>4</sub>Mn<sub>0.5</sub>Al-LDH, (d) re-Ca<sub>4</sub>Mn<sub>0.8</sub>Al-LDH, (e) re-Ca<sub>4</sub>Mn<sub>1.0</sub>Al-LDH and (f) re-Ca<sub>4</sub>Mn<sub>1.5</sub>Al-LDH recorded in 2170–2300 cm<sup>-1</sup> after CDCl<sub>3</sub> chemisorption at 25 °C.

Fourier-Transform infrared spectroscopy (FTIR), with deuterated chloroform (CDCl<sub>3</sub>, a weak acid) as probe molecule, was employed to study basic properties of solid materials under mild conditions.<sup>22–23</sup> For these re-Ca<sub>4</sub>Mn<sub>x</sub>Al-LDH samples, a broad FTIR band located in the range 2170–2300 cm<sup>-1</sup> is obtained and deconvoluted to four peaks *via* a Gaussian peak fitting method (Fig. 4). The two peaks at relatively high wavenumber (~2275 cm<sup>-1</sup> and ~2264 cm<sup>-1</sup>) are assigned to C–D stretching vibration of CDCl<sub>3</sub> gas and physically adsorbed CDCl<sub>3</sub>, respectively.<sup>24–25</sup> A red-shift magnitude relative to the CDCl<sub>3</sub> gas peak (~2275 cm<sup>-1</sup>) and the resulting proton affinities (calculated by eq. 1) are related to the Brønsted basic strength.<sup>26–27</sup> The deconvoluted FTIR spectra of all these samples display two bathochromic peaks with a maximum in the region 2251–2257 cm<sup>-1</sup> and 2214–2224 cm<sup>-1</sup>, which are identified as C–D stretching vibration of CDCl<sub>3</sub> adsorbed on weak basic site and on medium basic site, respectively.<sup>27–29</sup> According to the integral intensity of absorption bands of CDCl<sub>3</sub> on weak and medium basic sites, we compared re-Ca<sub>4</sub>Mn<sub>x</sub>Al-LDH samples in this

work with other types of LDHs, which were listed in Table S2. The results show for previously reported LDH samples, both weak basic site (proton affinity: 851–867 kJ/mol) and medium basic site (proton affinity: 919–931 kJ/mol) are observed. For re-Mg<sub>4</sub>Al-LDH samples, FTIR band at 2214 cm<sup>-1</sup> assigned to medium basic site (proton affinity: ~925 kJ/mol) is dominant, due to the presence of surface/interlayer hydroxyl group. In the case of re-Ca<sub>4</sub>Mn<sub>x</sub>Al-LDH samples however, FTIR band at 2256 cm<sup>-1</sup> corresponding to weak basic site (proton affinity: ~854 kJ/mol) is predominant, resulting from the seven-fold Ca–OH coordination. Based on our previous work,<sup>10</sup> we identified weak basic site with an FTIR band of adsorbed CDCl<sub>3</sub> at ~2255 cm<sup>-1</sup> and a proton affinity of ~855 kJ mol<sup>-1</sup>, and medium basic site with band at ~2214 cm<sup>-1</sup> and a proton affinity of ~925 kJ mol<sup>-1</sup>. Our previous work has also verified the weak basic site and medium basic site in re-Ca<sub>4</sub>Al-LDH material are derived from the active 7-fold Ca–OH coordination and physically-adsorbed surface hydroxyl group, respectively.<sup>10</sup> As shown in Fig. 4, for re-Ca<sub>4</sub>Al-LDH and the low Mn-containing samples (Mn/Al molar: 0.3, 0.5), it is observed that the weak basic site is dominant with almost constant intensity. A red shift from 2255 to 2257 cm<sup>-1</sup> is observed with the increase of Mn/Al molar ratio from 0 to 0.5, which indicates a further weakened weak basic site from 7-fold Ca–OH coordination structure (with proton affinity from 858 to 851 kJ mol<sup>-1</sup>), as a result of the influence of Ca–O–Mn<sup>IV</sup> structure.

Ca–O–Mn<sup>IV</sup> structure (as confirmed by EXAFS and XPS) in samples with a low content of Mn (Mn/Al molar: 0.3 and 0.5) induces a high s-orbital exposure of Ca<sup>2+</sup> and a strong interaction with the 7-fold OH<sup>-</sup>, resulting in a decreased electron density of hydroxyl oxygen and a weakened Brønsted basic site. In the case of samples with a high content of Mn (Mn/Al molar: 0.8, 1.0 and 1.5), the absorption band corresponding to weak basic site shifts to 2252 cm<sup>-1</sup> (proton affinity of 867 kJ mol<sup>-1</sup>) with an increased strength of weak base site, which indicates that the formation of Ca–O<sub>v</sub>–Mn<sup>III</sup> leads to an increased electron density of hydroxyl oxygen in 7-fold OH<sup>-</sup> and a rather strengthened Brønsted basic site. Meanwhile, the normalized peak area of medium basic site increases significantly. This indicates that Mn<sup>III</sup> and resulting Ca–O<sub>v</sub>–Mn<sup>III</sup> structure in high Mn-containing samples reduce the concentration of 7-fold Ca–OH coordination and facilitate the formation of physically-adsorbed surface hydroxyl, leading to less weak basic sites and more medium basic sites. Therefore, a controlled formation of Ca–O–Mn<sup>IV</sup> via changing the content of promoter Mn induces a high s-orbital exposure of Ca<sup>2+</sup> and a strong interaction with the 7-fold OH<sup>-</sup>, resulting in a decreased electron density of hydroxyl oxygen and a weakened Brønsted basic site; in contrast, the formation of Ca–O<sub>v</sub>–Mn<sup>III</sup> leads to an opposite effect and a rather strengthened Brønsted basic site.

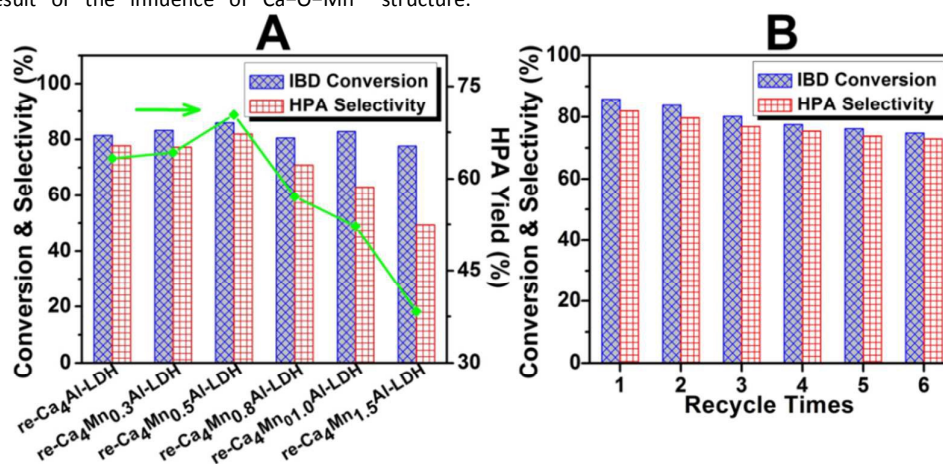


**Fig. 5** (A) IBD conversion, HPA selectivity and HPA yield over re-Ca<sub>4</sub>Mn<sub>x</sub>Al-LDH catalysts. (B) Catalytic behaviour of re-Ca<sub>4</sub>Mn<sub>0.5</sub>Al-LDH for 6 consecutive cycles. Reaction conditions: IBD (0.55 mmol), FA (0.80 mmol, 37% aqueous solution), cetyl trimethyl ammonium bromide (CTAB 0.1 g), dioxane (0.2 g), catalyst (0.2 g), 70 °C, 8 h, Ar atmosphere.

**Table 2.** Catalytic performances of various samples toward aldol condensation of isobutyraldehyde with formaldehyde<sup>a</sup>

Sample	Mn <sup>III</sup> /Mn <sup>IV</sup> molar ratios <sup>b</sup>	B <sub>w</sub> <sup>c</sup> (Area g <sup>-1</sup> )	B <sub>m</sub> <sup>c</sup> (Area g <sup>-1</sup> )	IBD Conversion (%)	HPA Selectivity (%)	HPA Yield (%)	Formation Rate <sup>d</sup> (mmol g <sup>-1</sup> h <sup>-1</sup> )
re-Ca <sub>4</sub> Al-LDH	/	44.65	10.26	81.4	77.8	63.3	57.1
re-Ca <sub>4</sub> Mn <sub>0.3</sub> Al-LDH	/	44.72	9.87	83.2	77.3	64.3	69.5
re-Ca <sub>4</sub> Mn <sub>0.5</sub> Al-LDH	0.407	46.18	9.56	85.9	81.9	70.3	98.0
re-Ca <sub>4</sub> Mn <sub>0.8</sub> Al-LDH	0.588	50.67	48.00	80.5	70.8	57.1	49.5
re-Ca <sub>4</sub> Mn <sub>1.0</sub> Al-LDH	0.688	24.82	64.33	82.8	63.1	52.2	34.3
re-Ca <sub>4</sub> Mn <sub>1.5</sub> Al-LDH	0.789	15.67	150.00	77.7	49.3	38.3	21.0

<sup>a</sup> Reaction conditions: isobutyraldehyde (0.55 mol), formaldehyde (0.80 mol), cetyl trimethyl ammonium bromide (0.1 g), dioxane (0.2 g), catalyst (0.2 g), 70 °C, 8 h, Ar atmosphere. <sup>b</sup> Mn<sup>III</sup>/Mn<sup>IV</sup> is calculated by the normalized XPS peak area assigned to Mn<sup>III</sup> and Mn<sup>IV</sup>, respectively, according to each integral area divided by sample quantity. <sup>c</sup> B<sub>w</sub> and B<sub>m</sub> are calculated based on integral intensity of absorption bands of CDCl<sub>3</sub> on weak and medium basic sites divided by sample quantity, respectively. <sup>d</sup> Formation rate of hydroxypivaldehyde (HPA) is calculated on the basis of tangent slope of the yield-reaction time plot at the 2% yield of HPA.

### 3.3 Catalytic performance evaluations

The aldol condensation of isobutyraldehyde (IBD) with formaldehyde (FA) to produce hydroxypivaldehyde (HPA, an intermediate in the production of neopentyl glycol) is a base-catalysed reaction with great industrial importance, which requires efficient heterogeneous catalysts for a “green” synthetic route.<sup>30</sup> In this work, the aldol condensation of IBD with FA was performed over these rehydrated LDH solid basic catalysts, and the catalytic evaluation data are shown in Fig. 5A and Table 2. With the increase of Mn/Al molar ratio, the equilibrium conversion maintains at ~80%; while the selectivity increases markedly at first and then decreases, and the maximal value (81.9%) is obtained over re-Ca<sub>4</sub>Mn<sub>0.5</sub>Al-LDH catalyst with a maximal yield of 70.3%. The results show that re-Ca<sub>4</sub>Mn<sub>x</sub>Al-LDH catalysts exhibit largely enhanced performance (HPA yield: 49–82%) in comparison with the Ca<sub>4</sub>Mn<sub>x</sub>Al-LDH precursors (HPA yield: 28–32%) or Ca<sub>4</sub>Mn<sub>x</sub>Al-MMOs (HPA yield: 20–37%) (Table S3). A comparison study between re-Ca<sub>4</sub>Mn<sub>0.5</sub>Al-LDH and previously reported catalysts toward the synthesis of HPA is performed, and the results show the largest HPA yield demonstrated in this work (Table S4). Most importantly, the catalytic behaviour of re-Ca<sub>4</sub>Mn<sub>0.5</sub>Al-LDH in this work, exceeds conventional solid base catalysts (33.4%) and is rather close to liquid alkali catalysts (73.2%) (see Table S3 for a systematic comparison). When the re-Ca<sub>4</sub>Mn<sub>0.5</sub>Al-LDH catalyst was reused for 6 consecutive cycles, both the conversion and yield decreased by ~5% after the firstly 4 consecutive cycles, and then maintained at a stable level within 5–6 cycles (Fig. 5B).

In order to investigate the promotion effect of Mn on rehydrated CaAl-hydroxalcalite catalysts, the yield of HPA vs. reaction time and initial formation rate at 2% IBD conversion that reflects the intrinsic catalytic property, are shown in Fig. 6A. For all these samples, HPA yield increases gradually along with reaction time and reaches the equilibrium maximum at 8 h. The largest equilibrium yield is present in the sample of re-Ca<sub>4</sub>Mn<sub>0.5</sub>Al-LDH

(70.3%). In addition, the formation rate of product (Fig. S5) follows a similar change tendency, and re-Ca<sub>4</sub>Mn<sub>0.5</sub>Al-LDH exhibits the maximal value (98 mmol g<sup>-1</sup>h<sup>-1</sup>). Meanwhile, some byproducts from Cannizzaro reaction or deep condensation are detected by HPLC-MS, including major neopentyl glycol, minor 3-hydroxy-2,2,4-trimethyl-pentanal and polymerization products. Our previous work has shown that weak Brønsted basic site (7-fold Ca–OH coordination) in rehydrated CaAl-LDHs serves as active centre to catalyse the aldol condensation, which accelerates the product desorption and thus promotes the HPA selectivity; therefore, tuning the strength and/or concentration of weak Brønsted base structure would play a key role in improving the selectivity toward aldol condensation product. Herein, to study the promotion effect of promoter Mn on catalytic performance of re-Ca<sub>4</sub>Mn<sub>x</sub>Al-LDH samples, the initial formation rate of HPA vs. relative concentration of Mn<sup>IV</sup> species (Mn<sup>IV</sup>/(Mn<sup>III</sup>+Mn<sup>IV</sup>)) or relative concentration of weak basic site (B<sub>w</sub>/(B<sub>w</sub>+B<sub>m</sub>)) (based on the normalized XPS or FTIR peak area listed in Table 2) for these re-Ca<sub>4</sub>Mn<sub>x</sub>Al-LDH catalysts are displayed in Fig. 6B and 6C, respectively. A linear correlation between initial formation rate and the relative concentration of Mn<sup>IV</sup> is observed (Fig. 6B), which manifests that Mn<sup>IV</sup> (Ca–O–Mn<sup>IV</sup> structure) serving as promoter improves the catalytic performance in aldol condensation reaction, other than the Mn<sup>III</sup> site (Ca–O<sub>v</sub>–Mn<sup>III</sup> structure). On the other hand, as shown in Fig. 6C, for low Mn-containing samples, the relative concentration of B<sub>w</sub> remains unchanged but initial formation rate increases significantly; however, in the case of the high Mn-containing samples, both the relative concentration of B<sub>w</sub> and initial formation rate decreases markedly with the increment of Mn content. This demonstrates that Mn<sup>IV</sup> (Ca–O–Mn<sup>IV</sup>) in low Mn-containing samples further decreases the strength of weak basic site, which accelerates the product desorption and largely promotes the HPA selectivity. For the high Mn-containing samples, Mn<sup>III</sup> (Ca–O<sub>v</sub>–Mn<sup>III</sup>) would decrease the concentration of 7-fold Ca–OH coordination and thus reduce the content of active site (weak basic sites), resulting in a low initial formation rate. The

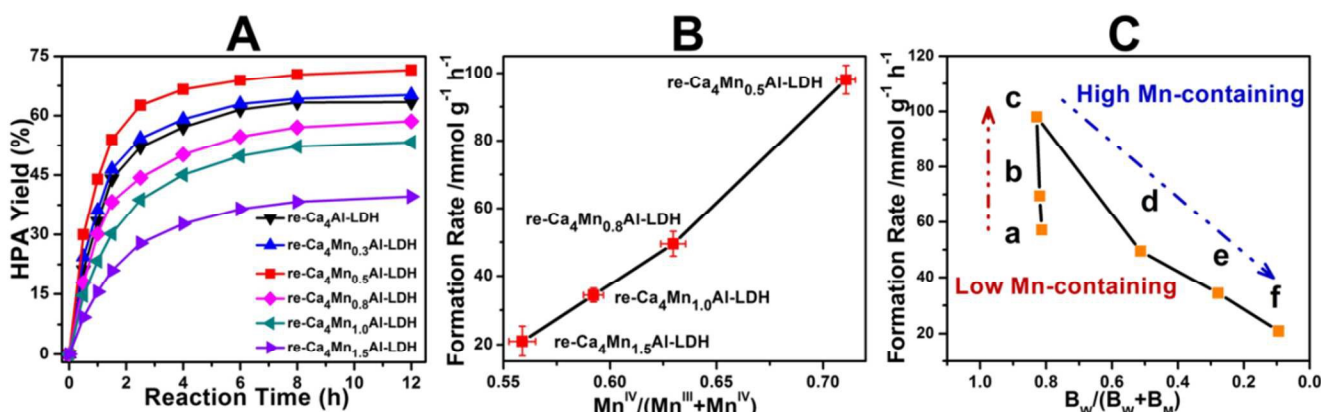


**Fig. 6** (A) Profiles of HPA yield vs. reaction time over re-Ca<sub>4</sub>Mn<sub>x</sub>Al-LDH catalysts. (B) Formation rate of HPA as a function of the normalized FTIR peak area assigned to relative concentration of Mn<sup>IV</sup> (Mn<sup>IV</sup>/(Mn<sup>III</sup>+Mn<sup>IV</sup>)). (C) Formation rate of HPA as a function of the normalized FTIR peak area assigned to weak basic site (B<sub>w</sub>/(B<sub>w</sub>+B<sub>m</sub>)) over (a) re-Ca<sub>4</sub>Al-LDH, (b) re-Ca<sub>4</sub>Mn<sub>0.3</sub>Al-LDH, (c) re-Ca<sub>4</sub>Mn<sub>0.5</sub>Al-LDH, (d) re-Ca<sub>4</sub>Mn<sub>0.8</sub>Al-LDH, (e) re-Ca<sub>4</sub>Mn<sub>1.0</sub>Al-LDH, and (f) re-Ca<sub>4</sub>Mn<sub>1.5</sub>Al-LDH, respectively.

## ARTICLE

results demonstrate that the electronic effect imposed by  $\text{Mn}^{\text{IV}}$  ( $\text{Ca-O-Mn}^{\text{IV}}$ ) modifies the 7-fold  $\text{Ca-OH}$  coordination, which causes a strengthened  $\text{Ca}^{2+}/\text{OH}^-$  interaction and a decreased strength of weak basic site, as confirmed by EXAFS, XPS and FTIR. This tuned weak basic site promotes HPA desorption and inhibits its deep condensation, which is responsible for the largely enhanced HPA selectivity in the sample of re- $\text{Ca}_4\text{Mn}_{0.5}\text{Al-LDH}$ .

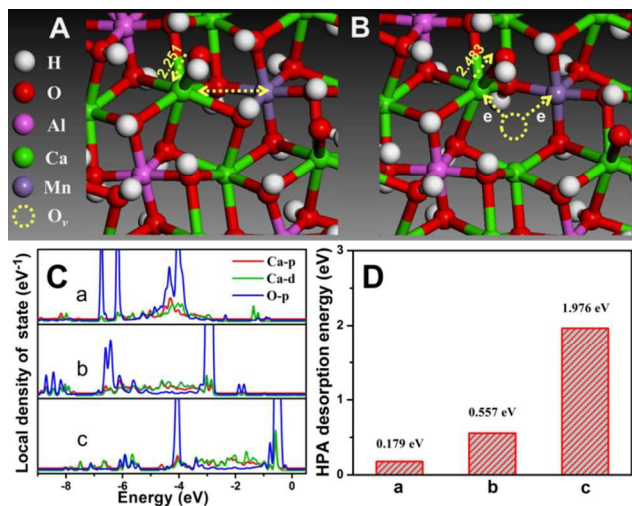


**Fig. 7** Schematic view of (A) optimized  $\text{Ca-O-Mn}^{\text{IV}}$  and (B)  $\text{Ca-O-Mn}^{\text{III}}$  based on DFT calculations. The hydroxyl in 7-fold  $\text{Ca-OH}$  coordination for  $\text{Ca-O-Mn}^{\text{IV}}$  system moves inward to Ca atom, and that for  $\text{Ca-O-Mn}^{\text{III}}$  system moves outward. (C) Local density of states (LDOS) of Ca and O atom in 7-fold  $\text{Ca-OH}$  coordination and (D) adsorption energies of HPA molecule in the system of: (a)  $\text{Ca-O-Mn}^{\text{IV}}$ , (b)  $\text{Ca-O-Al}$  and (c)  $\text{Ca-O-Mn}^{\text{III}}$ , respectively.

To further understand the promotion effect of Mn on rehydrated  $\text{CaAl}$ -hydroxalcalite catalysts, density functional theory (DFT) calculations were performed. As shown in Fig. 7A and 7B, the structural models of  $\text{Ca-O-Mn}^{\text{IV}}$  and  $\text{Ca-O-Mn}^{\text{III}}$  structure are built according to their XRD patterns, including a targeted Ca atom, Mn atom and several circumjacent O atoms in  $\text{Ca-O-M}$  octahedra and 7-fold  $\text{Ca-OH}$  coordination. In the optimized  $\text{Ca-O-Mn}^{\text{IV}}$  model (Fig. 7A), an obvious lattice expansion of  $\text{Ca-O-Mn}^{\text{IV}}$  octahedron with a  $\text{Ca-O-Mn}^{\text{IV}}$  bond length of 3.184 Å is found, larger than that of  $\text{Ca-O-Al}$  (3.134 Å). Otherwise, a shorter  $\text{Ca-O}$  bond length (2.251 Å) for 7-fold  $\text{Ca-OH}$  coordination is also observed, compared with  $\text{Ca-O-Al}$  structure (2.361 Å). The results confirm that the lattice expansion induces an enhanced exposure of  $\text{Ca}^{2+}$   $s$ -orbital and thus strengthens the interaction between  $\text{Ca}^{2+}$  and the 7-fold  $\text{OH}^-$ , in accordance with Ca K-edge EXAFS results. In the case of  $\text{Ca-O-Mn}^{\text{III}}$  system however (Fig. 7B), we found a longer  $\text{Ca-O}$  bond length (2.483 Å) in 7-fold  $\text{Ca-OH}$ , which is attributed to the lower exposure of  $\text{Ca}^{2+}$   $s$ -orbital and a weaker  $\text{Ca}^{2+}/7\text{-fold OH}^-$  interaction. The local density of states (Fig. 7C) was calculated to understand the interaction between Ca atom and O atom in 7-fold  $\text{Ca-OH}$ . For  $\text{Ca-O-Mn}^{\text{IV}}$ , the four main peaks of  $p$ -orbitals associated with O atom show a strong hybridization with the  $p$  and  $d$  orbitals of Ca atom, indicating a strong  $\text{Ca-O}$  interaction. For  $\text{Ca-O-Al}$  and  $\text{Ca-O-Mn}^{\text{III}}$ , the hybridization from

$p$ -orbitals of O atom decreases to three main peaks with a slight overlap with Ca atom, accounting for the weakened interaction between  $\text{Ca}^{2+}$  and the 7-fold  $\text{OH}^-$ , in agreement with the results of Ca K-edge EXAFS. In addition, based on catalytic evaluations in this work, we found that the equilibrium conversion of all catalysts maintains a high level at ~80%, but re- $\text{Ca}_4\text{Mn}_{0.5}\text{Al-LDH}$  sample with decreased strength of weak basic site exhibits the largest HPA selectivity and initial formation rate. The aldol condensation of IBD and FA to produce HPA is a classical one-step C-C coupling reaction, and deep condensation of HPA is the main side reaction; therefore, timely desorption of HPA from active site is the selectivity-determining step. A weak basic site is prone to release and transfer  $\text{H}^+$  to deprotonated HPA, which facilitates the desorption of HPA. To further confirm this conclusion, the desorption behaviour of HPA from  $\text{Ca-O-Mn}^{\text{IV}}$ ,  $\text{Ca-O-Al}$  or  $\text{Ca-O-Mn}^{\text{III}}$  was studied (Fig. 7D). The result reveals HPA desorption energy from  $\text{Ca-O-Mn}^{\text{IV}}$  is 0.179 eV, significantly lower than that from  $\text{Ca-O-Al}$  (0.557 eV) and  $\text{Ca-O-Mn}^{\text{III}}$  (1.976 eV), which is responsible for the largely enhanced HPA yield over the re- $\text{Ca}_4\text{Mn}_{0.5}\text{Al-LDH}$  catalyst.

## 4. Conclusions

In summary, rehydrated  $\text{CaMnAl}$ -layered double hydroxides (LDHs) as a heterogeneous basic catalyst were prepared based on the memory effect of LDH precursors. The resulting re- $\text{Ca}_4\text{Mn}_{0.5}\text{Al-LDH}$  exhibits a largely enhanced catalytic performance toward aldol condensation of isobutyraldehyde with formaldehyde (HPA yield of 70.3%), rather close to the level of liquid alkali catalysts (73.2%). A combination study including XPS, EXAFS and deuterated chloroform-FTIR spectra verifies that re- $\text{Ca}_4\text{Mn}_{0.5}\text{Al-LDH}$  contains a highly-exposed  $\text{Ca}^{2+}$   $s$ -orbital and strengthened coordination between  $\text{Ca}^{2+}$  and 7-fold  $\text{OH}^-$ , providing a weakened Brønsted basic site compared with the reference sample re- $\text{Ca}_4\text{Al-LDH}$ . Studies on the structure-property correlation based on experimental investigation and DFT calculation reveal that the decreased strength of weak Brønsted basic site modified by  $\text{Mn}^{\text{IV}}$  further accelerates the product desorption, accounting for the largely promoted HPA selectivity. This work provides a facile and cost effective approach for the preparation of LDHs-based solid basic catalysts with high performance, which can be used as a promising candidate in green catalysis of aldol condensation reactions.

## Acknowledgment

This work was supported by the National Key Research and Development Programme (Grant No. 2017YFA0206804), the National Natural Science Foundation of China (NSFC) and the Fundamental Research Funds for the Central Universities (buctylkxj01).

## Notes and references

## journal name

- S. Herrmann and E. Iglesia, *J. Catal.*, 2017, **346**, 134–153.
- R. Lee, J. R. Vanderveen, P. Champagne and P. G. Jessop, *Green Chem.*, 2016, **18**, 5118–5121.
- G. Liang, A. Wang, X. Zhao, N. Lei and T. Zhang, *Green Chem.*, 2016, **18**, 3430–3438.
- G. Busca, *Chem. Rev.*, 2010, **110**, 2217–2249.
- H. Hattori, *Appl. Catal., A*, 2015, **504**, 103–109.
- O. Kikhtyanin, R. Bulánek, K. Frolich, J. Čejka and D. Kubička, *J. Mol. Catal. A*, 2016, **424**, 358–368.
- L. Zhu, X. Q. Liu, H. L. Jiang and L. B. Sun, *Chem. Rev.*, 2017, **117**, 8129–8176.
- J. Yang, N. Li, S. Li, W. Wang, L. Li, A. Wang, X. Wang, Y. Cong and T. Zhang, *Green Chem.*, 2014, **16**, 4879–4884.
- R. Chaudhary and P. L. Dhepe, *Green Chem.*, 2017, **19**, 778–788.
- W. Bing, L. Zheng, S. He, D. Rao, M. Xu, L. Zheng, B. Wang, Y. Wang and M. Wei, *ACS Catal.*, 2017, **8**, 656–664.
- D. B. Rice, G. B. Wijeratne and T. A. Jackson, *J. Biol. Inorg. Chem.*, 2017, **22**, 1281–1293.
- Y. Melikhov, P. Konstantynov, J. Domagala, J. Sadowski, M. Chernyshova, T. Wojciechowski, Y. Syryanyy and I. N. Demchenko, *J. Phys.: Conf. Ser.*, 2016, **712**, 012114.
- A. W. Stubbs, L. Braglia, E. Borfecchia, R. J. Meyer, Y. Román-Leshkov, C. Lamberti and M. Dincă, *ACS Catal.*, 2017, **8**, 596–601.
- R. Chatterjee, G. Han, J. Kern, S. Gul, F. D. Fuller, A. Garachtchenko, I. D. Young, T.-C. Weng, D. Nordlund, R. Alonso-Mori, U. Bergmann, D. Sokaras, M. Hatakeyama, V. K. Yachandra and J. Yano, *Chem. Sci.*, 2016, **7**, 5236–5248.
- A. V. Soldatova, C. A. Romano, L. Tao, T. A. Stich, W. H. Casey, R. D. Britt, B. M. Tebo and T. G. Spiro, *J. Am. Chem. Soc.*, 2017, **139**, 11381–11391.
- F. H. Martins, F. G. Silva, F. L. O. Paula, J. de A. Gomes, R. Aquino, J. Mestnik-Filho, P. Bonville, F. Porcher, R. Perzynski and J. Depeyrot, *J. Phys. Chem. C*, 2017, **121**, 8982–8991.
- Y. Du, Q. Wang, X. Liang, Y. He, J. Feng and D. Li, *J. Catal.*, 2015, **331**, 154–161.
- J. Zhou, L. Qin, W. Xiao, C. Zeng, N. Li, T. Lv and H. Zhu, *Appl. Catal., B*, 2017, **207**, 233–243.
- J. Wang, J. Li, C. Jiang, P. Zhou, P. Zhang and J. Yu, *Appl. Catal., B*, 2017, **204**, 147–155.
- L. Zhu, J. Wang, S. Rong, H. Wang and P. Zhang, *Appl. Catal., B*, 2017, **211**, 212–221.
- G. Zhu, J. Zhu, W. Jiang, Z. Zhang, J. Wang, Y. Zhu and Q. Zhang, *Appl. Catal., B*, 2017, **209**, 729–737.
- M. N. Timofeeva, V. N. Panchenko, A. Gil, V. P. Doronin, A. V. Golovin, A. S. Andreev and V. A. Likholobov, *Appl. Catal., B*, 2011, **104**, 54–63.
- J. S. Valente, H. Pfeiffer, E. Lima, J. Prince and J. Flores, *J. Catal.*, 2011, **279**, 196–204.
- I. D. Ivanchikova, I. Y. Skobelev, N. V. Maksimchuk, E. A. Paukshtis, M. V. Shashkov and O. A. Kholdeeva, *J. Catal.*, 2017, **356**, 85–99.
- M. N. Timofeeva, V. N. Panchenko, J. W. Jun, Z. Hasan, M. M. Matrosova and S. H. Jhung, *Appl. Catal., A*, 2014, **471**, 91–97.
- C. Angelici, F. Meirer, A. M. J. van der Eerden, H. L. Schaink, A. Goryachev, J. P. Hofmann, E. J. M. Hensen, B. M. Weckhuysen and P. C. A. Bruijninx, *ACS Catal.*, 2015, **5**, 6005–6015.
- M. N. Timofeeva, V. N. Panchenko, A. Gil, Y. A. Chesalov, T. P. Sorokina and V. A. Likholobov, *Appl. Catal., B*, 2011, **102**, 433–440.
- M. N. Timofeeva, Z. Hasan, A. Y. Orlov, V. N. Panchenko, Y. A. Chesalov, I. E. Soshnikov and S. H. Jhung, *Appl. Catal., B*, 2011, **107**, 197–204.
- M. N. Timofeeva, A. E. Kapustin, V. N. Panchenko, E. O. Butenko, V. V. Krupskaya, A. Gil, M. A. Vicente, *J. Mol. Catal. A*, 2016, **423**, 22–30.
- H. Kleineberg, M. Eisenacher, H. Lange, H. Strutz and R. Palkovits, *Catal. Sci. Technol.*, 2016, **6**, 6057–6065.

## CaMnAl-hydrotalcite solid basic catalyst toward aldol condensation reaction with a comparable level to liquid alkali catalysts

Wei Han Bing,<sup>1</sup> Huimin Wang,<sup>1</sup> Lei Zheng,<sup>2</sup> Deming Rao,<sup>1</sup> Yusen Yang,<sup>1</sup> Lirong Zheng,<sup>\*2</sup>

Bin Wang,<sup>3</sup> Yangdong Wang,<sup>\*4</sup> Min Wei<sup>\*1</sup>

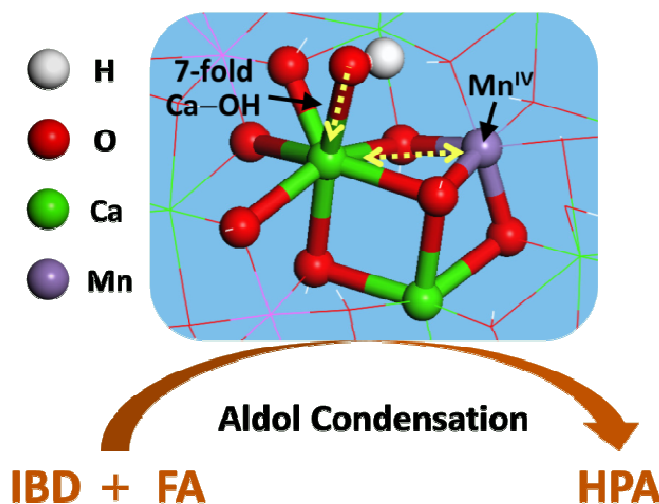
<sup>1</sup> State Key Laboratory of Chemical Resource Engineering, Beijing Advanced Innovation Center for Soft Matter Science and Engineering, Beijing University of Chemical Technology, Beijing 100029, P. R. China

<sup>2</sup> Institute of High Energy Physics, the Chinese Academy of Sciences, Beijing 100049, P. R. China

<sup>3</sup> Beijing Research Institute of Chemical Industry, Sinopec Group, Beijing 100013, P. R. China

<sup>4</sup> SINOPEC Shanghai Research Institute of Petrochemical Technology, Shanghai 201208, P. R. China

### Graphical Abstract



A CaMnAl-hydrotalcite solid basic catalyst was prepared based on the memory effect of LDHs, which exhibited extremely high catalytic performance toward aldol condensation reaction, comparable to level of liquid alkali catalysts.